

Superfluid Dynamics of a Bose-Einstein Condensate in a Periodic Potential

C. Menotti^{1,2}, A. Smerzi^{1,3} and A. Trombettoni⁴

¹ *Istituto Nazionale di Fisica per la Materia BEC-CRS and Dipartimento di Fisica, Università di Trento, I-38050 Povo, Italy*

² *Dipartimento di Matematica e Fisica, Università Cattolica del Sacro Cuore, I-25121 Brescia, Italy*

³ *Theoretical Division, Los Alamos National Laboratory, Los Alamos, NM 87545, USA*

⁴ *Istituto Nazionale per la Fisica della Materia and Dipartimento di Fisica, Università di Parma, parco Area delle Scienze 7A, I-43100 Parma, Italy*

(October 30, 2018)

We investigate the superfluid properties of a Bose-Einstein condensate (BEC) trapped in a one dimensional periodic potential. We study, both analytically (in the tight binding limit) and numerically, the Bloch chemical potential, the Bloch energy and the Bogoliubov dispersion relation, and we introduce *two* different, density dependent, effective masses and group velocities. The Bogoliubov spectrum predicts the existence of sound waves, and the arising of energetic and dynamical instabilities at critical values of the BEC quasi-momentum which dramatically affect its coherence properties. We investigate the dependence of the dipole and Bloch oscillation frequencies in terms of an effective mass averaged over the density of the condensate. We illustrate our results with several animations obtained solving numerically the time-dependent Gross-Pitaevskii equation.

I. INTRODUCTION

The study of the superfluid properties of Bose-Einstein condensates (BECs) trapped in periodic potentials are attracting a fast growing interest. The main reason is that the control parameters of such systems are widely tunable in realistic experiments, allowing for the investigation of different and fundamental issues of quantum mechanics, ranging from quantum phase transitions [1] and atom optics [2,3] to the dynamics of Bloch and Josephson oscillations [4–6]. Several efforts are also focusing on the realization of new technological devices as BEC interferometers working at the Heisenberg limit [3], and quantum information processors [2].

The dynamics of BECs in lattices is highly non-trivial, essentially because of the competition/interplay between the *discrete* translational invariance of the periodic potential and the *nonlinearity* arising from the interatomic interactions. For deep enough optical potentials, interactions induce a quantum transition from the superfluid to a Mott-insulator phase [1,7,8]. In this work we will study the system in a region of parameters such that its ground state stands deeply in the superfluid phase, with the dynamics governed by the Gross-Pitaevskii equation (GPE). Because of the discrete translational invariance, the excitation spectrum of the system exhibits a band structure which has several analogies with the electron Bloch bands in metals [9–11]. On the other hand, the coexistence of Bloch bands and nonlinearity allows, for instance, solitonic structures [12–14] and dynamical instabilities [15–17] which do not have an analog neither in metals, nor in Galilean invariant systems.

Exact, time-dependent solutions of the GPE with an external periodic potential, Eq.(1), can be written as Bloch states, namely as plane waves modulated by functions having the same periodicity of the lattice. The dynamics of small amplitude perturbations on top of these states satisfies two coupled, linear Bogoliubov equations, which can be solved numerically. However, when the interwell barriers of the periodic potential are high enough, the system can be described in a nonlinear tight binding approximation and several important properties of the system can be retrieved analytically [18]. Indeed, in the nonlinear tight binding approximation the continuous Gross-Pitaevskii equation can be replaced with a discrete nonlinear equation (DNL), Eq.(5), where the relevant observables of the system are the number of particles $N_l(t)$ trapped in well l and the relative phases $\phi_{l,l+1}(t) = \phi_{l+1}(t) - \phi_l(t)$. In this paper, we rewrite the results derived in [18] in a more convenient form, namely in terms of *two* effective masses and group velocities. Furthermore, we compare our analytical expressions with full numerical solutions, and we extend our analysis to investigate the behaviour of the system at low optical potential depths, where the nonlinear tight binding approximation breaks down. We show that the phenomena predicted by the DNL equation (5) can be generalized to the case of shallow potentials, bringing new insights on the dynamics of the system.

II. DISCRETE NONLINEAR DYNAMICS

In the “classical” (mean field) approximation, the BEC dynamics at $T = 0$ is governed by the Gross-Pitaevskii equation [19]

$$i\hbar \frac{\partial \Psi}{\partial t}(\vec{r}, t) = \left[-\frac{\hbar^2 \nabla^2}{2m} + V_{ext}(\vec{r}) + g |\Psi(\vec{r}, t)|^2 \right] \Psi(\vec{r}, t) = \mu \Psi(\vec{r}, t), \quad (1)$$

where $g = 4\pi\hbar^2 a/m$, with m the atomic mass and a the s -wave scattering length: $a > 0$ ($a < 0$) corresponds to an effective interatomic repulsion (attraction). In the following we consider only a BEC with repulsive interatomic interactions. The external potential V_{ext} includes the optical periodic potential V_P , which is typically superimposed to an harmonic (or linear) potential V_M . The periodic potential is

$$V_P = sE_R \sin^2\left(\frac{\pi x}{d}\right), \quad (2)$$

where d is the lattice spacing and π/d is the wavevector of the lasers in the lattice direction. The lattice spacing determines the Bragg momentum

$$q_B = \hbar \frac{\pi}{d}, \quad (3)$$

corresponding to the boundary of the first Brillouin zone. The energy barrier between adjacent sites is expressed in units of the recoil energy $E_R = q_B^2/2m$. From (2) we see that the minima of the laser potential are located at the positions $x_l = ld$ (l is an integer). Around these points, $V_P \approx m\tilde{\omega}_x^2(x - x_l)^2/2$, where $\hbar\tilde{\omega}_x = 2\sqrt{s}E_R$.

The harmonic potential is $V_M = m[\omega_x^2 x^2 + \omega_y^2 y^2 + \omega_z^2 z^2]/2$. Since, typically, $\omega_x \ll \tilde{\omega}_x$, it is convenient to write the external potential as $V_{ext} = V_L + V_D$, where the lattice potential $V_L = sE_R \sin^2(\pi x/d) + m[\omega_y^2 y^2 + \omega_z^2 z^2]/2$ includes the transverse confining field, and the “driving” field $V_D = m\omega_x^2 x^2/2$ gives the effective force acting on the center of mass of the condensate wave packet.

In order to understand the basic physics of the system, we first consider the case of deep optical lattices, where analytic solutions can be obtained in the tight binding approximation. Then we study the behaviour of the system beyond the tight binding limit, solving numerically the Gross-Pitaevskii and Bogoliubov equations with arbitrarily shallow periodic potentials.

As it has been previously shown in [18], when the interwell barriers are much higher than the chemical potential, it is possible to write the condensate wavefunction as

$$\Psi(\vec{r}, t) = \sum_l \psi_l(t) \Phi_l(\vec{r}; N_l(t)), \quad (4)$$

where the Wannier wavefunctions Φ_l are well localized in each well. The total number of atoms is $N_T = \sum_l N_l \equiv \sum_l |\psi_l|^2$. Replacing this Ansatz in the Gross-Pitaevskii equation (1) and integrating out the spatial degrees of freedom, we find the DNL equation

$$i\hbar \frac{\partial \psi_l}{\partial t} = \mathcal{V}_l \psi_l + \mu_l^{loc} \psi_l - \chi [\psi_l(\psi_{l+1}^* + \psi_{l-1}^*) + c.c.] \psi_l + \\ - [K + \chi (|\psi_l|^2 + |\psi_{l+1}|^2)] \psi_{l+1} - [K + \chi (|\psi_l|^2 + |\psi_{l-1}|^2)] \psi_{l-1}. \quad (5)$$

The “local” chemical potential μ_l^{loc} is the sum of three contributions

$$\mu_l^{loc} = \mu_l^{kin} + \mu_l^{pot} + \mu_l^{int} = \int d\vec{r} \left[\frac{\hbar^2}{2m} (\vec{\nabla} \Phi_l)^2 + V_L \Phi_l^2 + g|\psi_l|^2 \Phi_l^4 \right], \quad (6)$$

which depend on the atom number N_l explicitly through $|\psi_l|^2$ and implicitly through the shape of the Φ_l 's. The tunneling rates $K_{l,l\pm 1}$ between the adjacent sites l and $l \pm 1$ are

$$K \simeq - \int d\vec{r} \left[\frac{\hbar^2}{2m} \vec{\nabla} \bar{\Phi}_l \cdot \vec{\nabla} \bar{\Phi}_{l\pm 1} + \bar{\Phi}_l V_{ext} \bar{\Phi}_{l\pm 1} \right], \quad (7)$$

where the on-site wavefunctions have been calculated with an average number of atoms per site, $N_0 = |\psi_0|^2$, namely $\Phi_l(N_l) \simeq \bar{\Phi}_l(N_0)$ (a discussion of the validity of this approximation is in [18]). On the same line, the coefficient χ is given by

$$\chi = -g \int d\vec{r} \bar{\Phi}_l^3 \bar{\Phi}_{l\pm 1}, \quad (8)$$

and the on-site energies \mathcal{V}_l , arising from any external potential superimposed to the optical lattice, are

$$\mathcal{V}_l = \int d\vec{r} V_D \bar{\Phi}_l^2, \quad (9)$$

such that $\mathcal{V}_l \propto l^2$ ($\mathcal{V}_l \propto l$) when the driving field is harmonic (linear).

The dependence of the local chemical potential on the number of atoms is affected by the effective dimensionality of the condensates trapped in each well of the lattice. This can be determined comparing the interaction chemical potential $\mu_l^{int} = |\psi_l|^2 g \int d\vec{r} \Phi_l^4$ and the three frequencies, $\tilde{\omega}_x, \omega_y, \omega_z$ obtained expanding the lattice potential around the minima of each well $V_L \simeq m[\tilde{\omega}_x^2(x - x_l)^2 + \omega_y^2 y^2 + \omega_z^2 z^2]/2$. For instance, when $\tilde{\omega}_x, \omega_y, \omega_z \gg \mu_l^{int}$, the spatial width of each trapped condensate does not depend (in first approximation) on the number of particles N_l in the same well, and the condensate wavefunction in each valley of the periodic potential is well approximated by a gaussian. We consider this as a $0D$ (zero-dimensional) case: then, the nonlinear tight binding approximation (4) reduces to the usual tight binding approximation $\Psi(\vec{r}, t) = \sum_l \psi_l(t) \Phi_l(\vec{r})$ [12]. The $1D$ case arises when two frequencies are larger than the interaction chemical potential. In this case the system realizes an array of weakly coupled cigar-shaped condensates, with Φ_l factorized as gaussians along the two tight directions and a Thomas-Fermi in the other direction. In the $2D$ case only one frequency is smaller than the local interaction chemical potential: we have an array of pancake-like condensates, with Φ_l factorized as a gaussian along the tight direction and a Thomas-Fermi in the two other directions. The $3D$ case is given by the condition $\mu_l^{int} \gg \tilde{\omega}_x, \omega_y, \omega_z$ and the wavefunction in the l th well Φ_l is simply given by a three-dimensional Thomas-Fermi function. The crucial point is that the effective dimensionality of the condensates gives a different scaling of the local interaction chemical potential (6) with the number of atoms

$$\mu_l^{loc} = U_\alpha |\psi_l|^\alpha, \quad (10)$$

with $\alpha = \frac{4}{2+D}$, where $D = 0, 1, 2, 3$, $|\psi_l|^2$ is the number of atoms in well l , and U_α is a constant which does not depend on the number of atoms nor on the site index. When $\chi N_0 \ll K$ and $D = 0$, the DNL equation (5) gives the discrete nonlinear Schrödinger equation [12].

III. EXCITATION SPECTRA

In this section we derive the Bloch and the Bogoliubov excitation spectra of the system in absence of any driving field ($\mathcal{V}_l = 0$). First we derive our results analytically in the tight binding approximation; then we solve the equations numerically for a wide set of parameters to extend our treatment beyond the tight binding regime.

A. Bloch energy, Bloch chemical potential, effective masses and group velocities

The Bloch states $\Psi_p(x) = e^{ipx/\hbar} \tilde{\Psi}_p(x)$, where $\tilde{\Psi}_p(x)$ is periodic with period d , are exact stationary solutions of the Gross-Pitaevskii equation (1). Both the energy per particle $\varepsilon_\alpha(p)$ (Bloch energy) and the chemical potential $\mu_\alpha(p)$ of such solutions form a band structure, so that they can be labeled by the quasi-momentum p and the band index α .

The DNL equation (5) describes only the lowest band of the spectrum (in the following, we will consider only the lowest band $\alpha = 1$, and we will omit, for simplicity, the band index α). Exact solutions of the DNL equation are the "plane waves" $\psi_l = \psi_0 e^{i(pld - \mu t)/\hbar}$, where p is the quasi-momentum, and l is the site index (note that the ψ_l are plane waves in the discrete l -space, but do not correspond to plane waves in real space). Within the DNL equation framework, the energy per particle $\varepsilon(p)$ and chemical potential $\mu(p)$ corresponding to these solutions are

$$\varepsilon(p) = \varepsilon^{loc} - 2 (K + 2 \chi N_0) \cos\left(\frac{\pi p}{q_B}\right) \equiv \varepsilon^{loc} - \frac{q_B^2}{\pi^2 m_\varepsilon} \cos\left(\frac{\pi p}{q_B}\right), \quad (11)$$

$$\mu(p) = \mu^{loc} - 2 (K + 4 \chi N_0) \cos\left(\frac{\pi p}{q_B}\right) \equiv \mu^{loc} - \frac{q_B^2}{\pi^2 m_\mu} \cos\left(\frac{\pi p}{q_B}\right), \quad (12)$$

where $\mu^{loc} = \mu_l^{loc}|_{\psi_l=\psi_0} = \partial(N_0 \varepsilon^{loc})/\partial N_0$, with $N_0 = |\psi_0|^2$ the number of atoms per well and $\varepsilon^{loc} = 2U_\alpha N_0^{\alpha/2}/(\alpha+2)$. In the previous equations we have introduced the effective masses m_ε and m_μ , to emphasize the low momenta (long wavelength) quadratic behaviour of the Bloch energy spectrum and of the chemical potential [20]. It turns out that several dynamical properties of the system can be intuitively understood in terms of such effective masses. This approach is quite common, for instance, in the theory of metals, where $m_\mu \equiv m_\varepsilon$. However in BEC, because of the nonlinearity of the Gross-Pitaevskii equation, the two relevant energies of the system, ε and μ , have the same $\cos(\pi p/q_B)$ dependence on the quasi-momentum p , but different curvatures. Therefore, $m_\mu \neq m_\varepsilon$, with

$$\frac{1}{m_\varepsilon} \equiv \left. \frac{\partial^2 \varepsilon}{\partial p^2} \right|_{p=0} = \frac{2\pi^2 (K + 2\chi N_0)}{q_B^2}, \quad (13)$$

$$\frac{1}{m_\mu} \equiv \left. \frac{\partial^2 \mu}{\partial p^2} \right|_{p=0} = \frac{2\pi^2 (K + 4\chi N_0)}{q_B^2}, \quad (14)$$

where K and χ have been defined in Eqs.(7,8). Sometimes it is convenient to extend the definition of the effective masses to the full Brillouin zone, introducing the quasi-momentum dependent masses

$$m_\varepsilon(p) \equiv \left[\frac{\partial^2 \varepsilon}{\partial p^2} \right]^{-1} = \frac{m_\varepsilon}{\cos(\pi p/q_B)}, \quad (15)$$

$$m_\mu(p) \equiv \left[\frac{\partial^2 \mu}{\partial p^2} \right]^{-1} = \frac{m_\mu}{\cos(\pi p/q_B)}, \quad (16)$$

where, following Eqs.(13,14), $m_\varepsilon = m_\varepsilon(0)$ and $m_\mu = m_\mu(0)$.

It is also useful to introduce, with the same line of reasoning, two different group velocities, defined as

$$v_\varepsilon \equiv \frac{\partial \varepsilon}{\partial p} = \frac{1}{m_\varepsilon} \frac{q_B}{\pi} \sin\left(\frac{\pi p}{q_B}\right), \quad (17)$$

$$v_\mu \equiv \frac{\partial \mu}{\partial p} = \frac{1}{m_\mu} \frac{q_B}{\pi} \sin\left(\frac{\pi p}{q_B}\right). \quad (18)$$

There is a simple, general relation between the two different group velocities (following from $\mu = \partial(N_0 \varepsilon)/\partial N_0$)

$$v_\mu = v_\varepsilon + \frac{\partial v_\varepsilon}{\partial N_0} N_0 \quad (19)$$

with, given Eqs.(13,14), $v_\mu > v_\varepsilon$. The analog relation for the effective masses has been retrieved in [20].

Of course, the concept of *effective mass*, defined as the inverse of the curvature of the corresponding spectrum (as that of *group velocity*, defined as the first derivative) can be extended to shallow optical potentials, where the nonlinear tight binding approximation breaks down. In this case, the quasi-momentum dependence of ε and μ will not be simply described by a cosine function, but will still remain periodic in the quasi-momentum p . In particular, the value p where $m_\varepsilon(p)$ changes sign (corresponding to $\partial^2 \varepsilon / \partial p^2 = 0$) will be greater than $q_B/2$ and will in general not coincide with the momentum where $m_\mu(p)$ changes sign (corresponding to $\partial^2 \mu / \partial p^2 = 0$).

The presence of the two *different* effective masses (group velocities) raises an important problem: which effective mass (group velocity), and how, enters in the dynamical properties of the system? For instance, we anticipate that the current carried by a Bloch waves with quasi-momentum p is $\rho_0 v_\varepsilon(p)$, where ρ_0 is the average particle density; m_μ , on the other hand, plays a crucial role in the Bogoliubov spectrum. To conclude this subsection, we notice that the Bloch states are not the only stationary solutions of the Gross-Pitaevskii equation. Because of nonlinearity, indeed, periodic solitonic solutions can also appear for a weak enough periodic potential, introducing new branches in the excitation spectra [21,22].

B. Bogoliubov dispersion relation

In this subsection we study the Bogoliubov spectrum of elementary excitations. This describes the energy of small perturbations with quasi-momentum q on top of a macroscopically populated state with quasi-momentum p (stationary solution of Eq.(1)). To be explicit, let us consider first the case in which the radial degrees of freedom y, z are integrated out. The wavefunction along the x direction can be written as

$$\Psi(x, t) = e^{-i\mu(p)t/\hbar} e^{ipx/\hbar} \left[\tilde{\Psi}_p(x) + \sum_q \tilde{u}_{pq}(x) e^{iqx/\hbar} e^{-i\omega_{pq}t} + \tilde{v}_{pq}^*(x) e^{-iqx/\hbar} e^{i\omega_{pq}t} \right]. \quad (20)$$

Because of the periodicity, the Bogoliubov amplitudes can be written as Bloch waves [i.e., $\{u, v\}_{pq}(x) = \exp(iqx/\hbar) \{\tilde{u}, \tilde{v}\}_{pq}(x)$], where q is the quasi-momentum of the excitation and $\{\tilde{u}, \tilde{v}\}_{pq}(x)$ are periodic functions. The subscript $\{pq\}$ indicates that both the amplitudes \tilde{u}, \tilde{v} and the excitation frequencies ω_{pq} depend on the quasi-momentum p of the carrying wave and on the quasi-momentum q of the excitation.

In terms of the periodic functions $\tilde{\Psi}$, \tilde{u} and \tilde{v} , the Bogoliubov equations take the form

$$\left[\frac{1}{2m} (-i\hbar\partial_x + p + q)^2 + s E_R \sin^2 \left(\frac{\pi x}{d} \right) - \mu + 2gnd|\tilde{\Psi}_p|^2 \right] \tilde{u}_{pq}(x) + gnd\tilde{\Psi}_p^2 \tilde{v}_{pq}(x) = \hbar\omega_{pq} \tilde{u}_{pq}(x) \quad (21)$$

$$\left[\frac{1}{2m} (-i\hbar\partial_x - p + q)^2 + s E_R \sin^2 \left(\frac{\pi x}{d} \right) - \mu + 2gnd|\tilde{\Psi}_p|^2 \right] \tilde{v}_{pq}(x) + gnd\tilde{\Psi}_p^{*2} \tilde{u}_{pq}(x) = -\hbar\omega_{pq} \tilde{v}_{pq}(x) \quad (22)$$

where n is the 3D-average density and $\int_{-d/2}^{d/2} |\tilde{\Psi}_p|^2 dx = 1$. Equations (21,22) can be solved numerically in a very efficient way working with the Fourier components of $\tilde{\Psi}$, \tilde{u} and \tilde{v} .

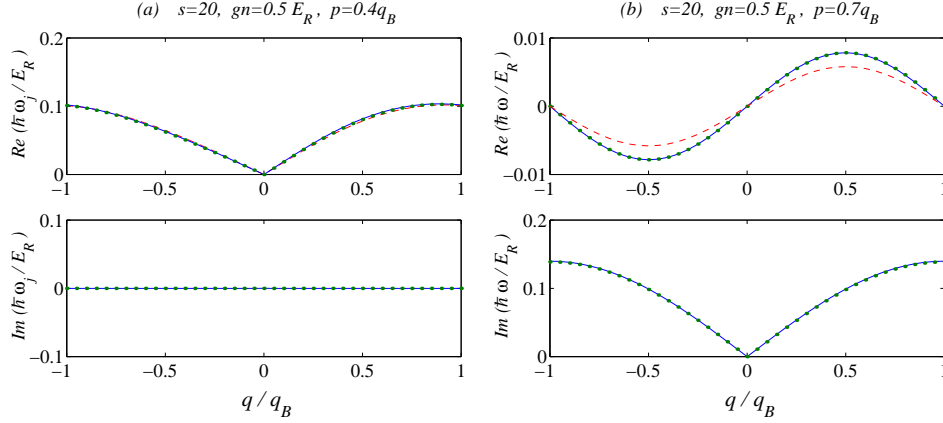


FIG. 1. Numerical solutions of Eqs.(21,22) for $s = 20$ and $gn = 0.5E_R$ (green dots); analytic solution Eq.(23) in the tight binding approximation (solid blue line); analytic solution of Eq.(23) where m_μ is replaced with m_ϵ (dashed red line). The quasi-momentum of the carrying wave is $p = 0.4q_B$ in (a) and $p = 0.7q_B$ in (b).

In the tight binding regime, the Bogoliubov analysis corresponds to perturbing the large amplitude wave as $\psi_l = [\psi_0 + \delta\psi_l] e^{i(pld - \mu t)/\hbar}$, with $\delta\psi_l = \sum_q \mathcal{U}_q e^{i(qld/\hbar - \omega_{pq}t)}$. Retaining only first order terms with respect to $\delta\psi$, we get two coupled linear equations analogous to (21) whose eigenvalues can be calculated analytically [18]. The general solution (for any effective dimensionality of the system: $D = 0, 1, 2, 3$) is

$$\begin{aligned} \hbar\omega_{pq} &= \frac{q_B^2}{\pi^2 m_\mu} \sin\left(\frac{\pi p}{q_B}\right) \sin\left(\frac{\pi q}{q_B}\right) \pm \\ &\pm 2\sqrt{\frac{q_B^4}{\pi^4 m_\mu^2} \cos^2\left(\frac{\pi p}{q_B}\right) \sin^4\left(\frac{\pi q}{2q_B}\right) + \frac{q_B^2}{\pi^2 m_\epsilon} \frac{\partial\mu}{\partial N_0} N_0 \cos\left(\frac{\pi p}{q_B}\right) \sin^2\left(\frac{\pi q}{2q_B}\right) +} \\ &+ O\left[\left(\frac{m_\mu^{-1} - m_\epsilon^{-1}}{m_\mu^{-1}}\right)^2\right] \end{aligned} \quad (23)$$

with the chemical potential given by $\mu(p, N_0) = \mu^{loc} - \frac{q_B^2}{\pi^2 m_\mu} \cos\left(\frac{\pi p}{q_B}\right)$ (see Eq.(12)), and $\mu_l^{loc} = U_\alpha | \psi_l |^{4/(2+D)}$. For $D = 0$ and in the limit $\chi = 0$, we recover the well-known results for the discrete nonlinear Schrödinger equation [16,24]. Equation (23) has been first written in [18] in terms of the parameter of the DNL equation Eq.(5), while, for small q and arbitrary p , has been derived in [17] for arbitrary values of s .

In Fig. 1, we compare the analytic results (dots) with the numerical solution of Eqs.(21,22) (solid line), for a system in tight binding regime. In the numerical calculations, the effective masses have been obtained from the curvatures of the Bloch energy and chemical potential spectra, while the term $N_0 \frac{\partial\mu}{\partial N_0}$ has been evaluated from the density dependence of the chemical potential. As it has already been noted in [20], effects related with the difference between the two effective masses in the Bogoliubov spectrum of a condensate at rest ($p = 0$) are usually negligible. On the contrary, such difference becomes important when the condensate moves with a large quasi-momentum, as shown in Fig. 1(b).

IV. SOUND WAVES & INSTABILITIES

The small q (large wavelength) limit of the Bogoliubov dispersion relation becomes

$$\hbar\omega_{pq} \approx \frac{q_B}{\pi m_\mu} \sin\left(\frac{\pi p}{q_B}\right) q + |q| \sqrt{\frac{1}{m_\varepsilon} \frac{\partial \mu}{\partial N_0} N_0 \cos\left(\frac{\pi p}{q_B}\right)}, \quad (24)$$

(we assume, for the moment, that $\frac{1}{m_\varepsilon} \frac{\partial \mu}{\partial N_0} N_0 \cos(\pi p/q_B) > 0$). The linear behaviour in q indicates that the system supports (low amplitude) sound waves, propagating on top of the large amplitude traveling wave Ψ_p with velocity

$$v_{s,\pm} = \hbar \frac{\partial \omega}{\partial q} \Big|_{q \rightarrow 0^\pm} = \begin{cases} v_\mu + c, & (q \rightarrow 0^+) \\ v_\mu - c, & (q \rightarrow 0^-) \end{cases} \quad (25)$$

where the “chemical potential group velocity” v_μ has been defined in Eq.(18), and the “relative sound velocity” c is defined as

$$c = \sqrt{\frac{1}{m_\varepsilon} \frac{\partial \mu}{\partial N_0} N_0 \cos\left(\frac{\pi p}{q_B}\right)}. \quad (26)$$

The two different velocities $v_{s,\pm}$ correspond, respectively, to a sound wave propagating in the same and in the opposite direction of the large amplitude traveling wave. As we have already noticed, and we will discuss again in the next section, v_μ is different from (it is larger than) the actual velocity of the large amplitude wave, see Eq.(19).

We remark that, contrary to the case of a Galilean invariant system ($s = 0$), the sound velocity depends on the quasi-momentum p . Moreover, v_s depends on the effective dimensionality of the condensates, since (from Eq.(10,12)) $\frac{\partial \mu}{\partial N_0} N_0 \sim \alpha U_\alpha N_0^{\alpha/2}$. In the limit $\alpha = 2$, $p \rightarrow 0$ and $m_\varepsilon, m_\mu \rightarrow m$ we get the sound velocity in the uniform case.

The system is energetically unstable if there exist any $\omega_{pq} < 0$. In the limit $s = 0$, this corresponds to a group velocity larger than the sound velocity (Landau criterion for superfluidity). When the system has a discrete translational invariance ($s > 0$) the condition for this instability is obtained from the Bogoliubov excitation spectrum Eq.(23). Then, we have that the system is not superfluid when $\omega_{pq} < 0$, corresponding to

$$v_\mu^2 > c^2. \quad (27)$$

This result should be compared with the well known Landau criteria for an homogeneous system ($s = 0$), stating that the superfluid is energetically unstable when $v^2 > c^2$, $v \equiv \frac{\partial \varepsilon}{\partial p} = \frac{\partial \mu}{\partial p}$ being the group velocity of the condensate, and $c = \sqrt{\frac{1}{m} \frac{\partial \mu}{\partial N_0} N_0}$ the sound velocity.

There is a further dynamical (modulational) instability mechanism associated with the appearance of an imaginary component in the Bogoliubov frequencies, which disappears in absence of interatomic interactions, or in the translational invariant limit (if $a > 0$). The onset of this instability in the tight binding regime, coincides with the condition

$$c^2 < 0 \Rightarrow \cos\left(\frac{\pi p}{q_B}\right) < 0 \Rightarrow |p| > \frac{q_B}{2}. \quad (28)$$

The dynamical instability drives an exponentially fast increase of the amplitude of the (initially small) fluctuations of the condensate. Since the initial phases and amplitudes of the fluctuation modes are essentially random, their growth induce a strong dephasing of the condensate, and dissipates its translational kinetic energy (which is transformed in incoherent collective and single particles excitations). The unstable modes q grow with a time scale given by the imaginary part of the excitation frequency

$$\tau_{pq}^{-1} = \frac{2q_B}{\pi \hbar} \left| \sin\left(\frac{\pi q}{q_B}\right) \right| \text{Im} \left[\sqrt{\frac{q_B^2}{\pi^2 m_\mu^2} \cos^2\left(\frac{\pi p}{q_B}\right) \sin^2\left(\frac{\pi q}{2q_B}\right) + \frac{1}{m_\varepsilon} \frac{\partial \mu}{\partial N_0} N_0 \cos\left(\frac{\pi p}{q_B}\right)} \right]. \quad (29)$$

We remark here the different scaling of the energetic and dynamical instability with the interatomic interactions. Decreasing the scattering length, the sound velocity decreases, and smaller and smaller group velocities can breakdown the superfluidity of the system (in the limit $a = 0$, the sound velocity $c = 0$: the non interacting condensate is always energetically unstable for an arbitrary small group velocity). On the other hand, the dynamical modulational

instability criteria does not depend on the scattering length. This apparent paradox is simply solved noticing that the growth time of the unstable modes, Eq.(29), actually depends on interactions, and diverge when the scattering length vanishes ($\tau \rightarrow \infty$ when $a \rightarrow 0$). Therefore, a noninteracting condensate is always dynamically stable. There is a further point to remark: if we consider a condensate moving with an increasing velocity, the system always becomes first energetically unstable, then it hits the dynamical instability. As a matter of fact, however, in real experiments the energetic instability can grow quite slowly (and at zero temperature only in presence of impurities [15]), so that the dominant dephasing mechanism is given by the modulational instability. This aspect can be highlighted also with numerical experiments, studying, for instance, Bloch oscillations of a condensate with the interactions switched off. In this case, even though the system is energetically unstable, it remains coherent over many oscillations. If the interatomic interactions are switched on, however, the system dephase rather quickly, the dephasing occurring when the quasi-momentum of the condensate is in the dynamical unstable region of the Bloch spectrum. We have done such numerical experiment, and results are shown in Movies 4 and 5. Of course, our prediction can be tested in real experiments, tuning the scattering length with a Feshbach resonance.

To summarize, the tight binding approximation predicts the arising of the dynamical instability (complex excitation frequency) for $p = q_B/2$. We point out that $p = q_B/2$ also corresponds to the quasi-momentum where, in the tight binding regime, the effective masses $m_\epsilon(p)$ and $m_\mu(p)$ change sign. A system with a negative effective mass and positive scattering length can be, roughly speaking, seen as equivalent to a system with a negative scattering length and positive effective mass. It is well known that a BEC having a negative scattering length is dynamically unstable, and, therefore, such parallelism could be proposed to give a simple explanation of the instability. However, we will see that this coincidence between the arising of dynamical instabilities and the inversion of sign of the effective mass does not take place at lower optical potentials (see Fig. 3).

Let us concentrate now on the behaviour of the excitation frequencies for shallow optical potentials, where the tight binding expression derived in (23) is not applicable. For small optical potential depths, the Bogoliubov equations have to be solved numerically and the results show a more complicated behaviour. In Movies 2(a-c), we show the numerical solutions of the 1D Bogoliubov equations for three different values of s ($s = 1, 2$ and 5). In those movies, we plot the real and imaginary part of ω_{pq} as a function of q and we vary p in time.

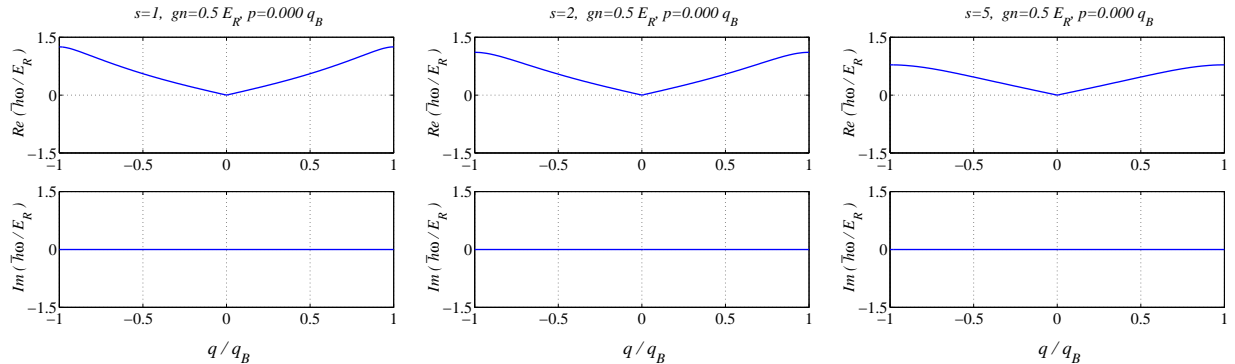


FIG. 2. MOVIES: Real and imaginary part of ω_{pq} as a function of q for different values p , for $gn = 0.5E_R$ and $s = 1$ (a), $s = 2$ (b) and $s = 5$ (c).

We point out a series of differences with respect to the tight binding regime:

- the complex frequencies appear at the boundary of the first Brillouin zone ($q = q_B$) for a value of $p > q_B/2$ (dots in Fig. 3) and they reach the center of the zone ($q = 0$) for a higher value of p (orange region in Fig. 3).
- the range of momenta p where the frequencies are complex for some q , but real around $q = 0$, decrease by increasing s . In the tight binding limit this range vanishes;
- in the limit of our numerical accuracy, which is due to the discrete sampling of p and q , we found that the value of p where the effective mass m_ϵ changes sign (squares in Fig. 3) corresponds to the value of p at which the frequencies with non vanishing imaginary part reach $q \approx 0$. In the tight binding approximation, this appears explicitly through the term $\cos(\pi p/q_B)/m_\epsilon$ under the square root.

We would like to remark two important results arising from our study of the excitation spectra. First, as shown in Fig.3, we found the onset of the dynamical instability for values of the quasi-momentum where the effective mass $m_\epsilon(p)$ is still positive. Second, the range of momenta where the system has a positive effective mass and, at the same time, is dynamically unstable, increases by decreasing s (keeping in mind that the amplitude of the imaginary part vanishes for $s \rightarrow 0$ or $gn \rightarrow 0$, which implies that the growth in time of the instability diverges both for uniform interacting systems and for an ideal gases in optical lattices). So, one can study the behaviour of the system at low

s to distinguish between two possible dephasing mechanisms, one due to the sign of m_ε , the other one due to the dynamical instability, as it will be extensively explained in Sect.VI.

We conclude this section remarking that various important aspects of the physics of energetic and dynamical instabilities of a BEC in a periodic potential have been studied in [12,15–17].

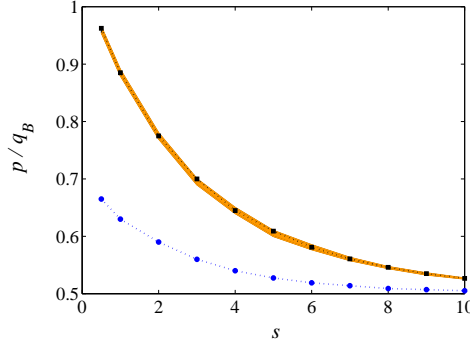


FIG. 3. Results from the numerical solution of Eqs.(21,22) for $gn = 0.5E_R$ as a function of s . Dots: value of the quasi-momentum p where the excitation frequencies $\omega_{pq}(q = \pm q_B)$ become complex; orange region: value of the quasi-momentum p where complex frequencies are found around $q = 0$; squares: value of the quasi-momentum p where the effective mass m_ε changes sign. The dotted lines are a guide to the eye.

V. NEWTONIAN DYNAMICS

Using the results in [18], we can now rewrite the dynamics of a BEC wave-packet in terms of the energy effective mass. For the BEC wave-packet we use the following ansatz

$$\psi_l = \sqrt{\mathcal{K}(\sigma)} f\left(\frac{l - \xi}{\sigma}\right) e^{iP(l - \xi) + i\frac{\delta}{2}(l - \xi)^2}, \quad (30)$$

where $\xi(t)$ and $\sigma(t)$ are, respectively, the center and the width (in lattice units) of the wavepacket, $P(t)$ and $\delta(t)$ their associated momenta and $\mathcal{K}(\sigma)$ a normalization factor such that $\sum_l N_l = N_T$ (with $|\psi_l|^2 \equiv N_l$). The function f is generic, for instance, we can choose $f(X) = e^{-X^2}$ or $f(X) = (1 - X^2)^{1/\alpha}$ (with $-1 \leq X \leq 1$) to describe, respectively, the dynamics of a gaussian or a Thomas-Fermi wavepacket. The equations of motion of the collective variables $\xi(t), \sigma(t), p(t), \delta(t)$ have been obtained in [12,18]. With $\mathcal{V}_j = \Omega j^2$ ($\Omega = md^2\omega_x^2/2$), and neglecting the dynamics wave-packet width dynamics ($\dot{\sigma}(t) = 0$), we find that the group velocity $\dot{\xi}$ and the effective force acting on the center of mass of the wavepacket are given by

$$\hbar \dot{\xi} = \frac{q_B^2}{\pi^2} \left\langle \frac{1}{m_\varepsilon} \right\rangle \sin P, \quad (31)$$

$$\hbar \dot{P} = -\frac{\partial V_d}{\partial \xi}, \quad (32)$$

where $V_d = \Omega(\xi^2 + \sigma^2 \frac{\mathcal{I}_2}{\mathcal{I}_1})$ with $\mathcal{I}_1 = \int dX f^2(X)$ and $\mathcal{I}_2 = \int dX X^2 f^2(X)$. Since the effective masses depend on the local (on-site) density, we have to introduce an effective mass averaged over the local density of the condensate wavepacket

$$\left\langle \frac{1}{m_\varepsilon} \right\rangle = \frac{\sum_l m_\varepsilon^{-1}(N_l) |\psi_l|^2}{\sum_l |\psi_l|^2}, \quad (33)$$

with, according to Eq.(13), $m_\varepsilon^{-1}(N_l) = (2\pi^2/q_B^2)(K + 2\chi N_l)$. We summarize here the most important results, written in term of the effective mass m_ε :

(i) in the case of an homogeneous system ($V_D = 0$, $N_l = \text{const.}$), the tunneling rate is given by

$$\frac{\pi^2 \hbar}{q_B^2} \frac{\dot{N}_l^{\text{out}}}{N_l \Delta \phi} |_{\Delta \phi \rightarrow 0} = \frac{1}{m_\varepsilon}; \quad (34)$$

(ii) the frequency of small amplitude oscillations of the wavepacket driven by an harmonic field $\mathcal{V}_l \propto l^2$ is

$$\frac{\omega_{dip}}{\omega_x} = \sqrt{\left\langle \frac{m}{m_\varepsilon} \right\rangle}; \quad (35)$$

(iii) if the driving field is linear $\mathcal{V}_l = mGdl$, we have simple Bloch oscillations with

$$\xi = \left\langle \frac{1}{m_\varepsilon} \right\rangle \frac{q_B^2}{\pi^2 m G d} \cos\left(\frac{\pi m G}{q_B} t\right). \quad (36)$$

This analysis does not take into account possible dephasing mechanisms as those investigated in the previous section. In the collective coordinate approach, such dephasing mechanisms can be described including the dynamics of the width of the wavepacket $\sigma(t)$ and of the corresponding momentum $\delta(t)$ [12].

VI. NUMERICAL EXPERIMENTS ON BLOCH OSCILLATIONS, DIPOLE OSCILLATIONS AND FREE EXPANSIONS IN THE LATTICE

In this section, we discuss some numerical simulations of the Gross-Pitaevskii equation in order to illustrate the phenomena described in the previous sections. We first consider Bloch oscillations (Sect. VI A): we create the condensate in a harmonic trap superimposed to the lattice and then switch off the harmonic trap and replace it with a linear potential. We expect that the BEC oscillates periodically in space (Bloch oscillations).

The second numerical simulation consists in creating the condensate in a harmonic trap superimposed to the lattice, and suddenly displacing the center of the harmonic trap (Sect. VI B). This experiment has already been studied theoretically [16] and performed experimentally in [6,23]. We discuss it again, generalizing the previous results to the case of shallow optical lattices.

The third numerical simulation consists in creating a condensate in a harmonic trap superimposed to the optical lattice and, thereafter, switching off the harmonic trap in the lattice direction, letting the condensate expand in the periodic potential (Sect. VI C): for values of the the mean-field energy large enough (with a fixed height s of the interwell energy barriers), the wave-packet is self-trapped [12] and the spreading of the wave packet does not occur.

In all cases, for an interacting BEC, we have found some sort of self-trapping and dynamical instabilities for some values of the depth of the periodic potential or the initial conditions of the BEC wave packet. For instance, in the dipole oscillation experiment, the condensate may stop on one side of the harmonic potential being unable to complete the oscillation. It is useful to look at the dynamical evolution of the relative phases of condensates trapped in neighboring wells and the BEC evolution in momentum space. There is a clear correspondence between the distribution in *momentum* space and that in *quasi-momentum* space: the quasi-momentum distribution of the Bloch state $\Psi_p(x) = e^{ipx/\hbar} \tilde{\Psi}_p(x)$ with quasi-momentum p is $\delta(p)$; its momentum distribution is $|\sum_\ell c_\ell \delta(p + 2\ell q_B)|^2$, where ℓ are integers and where the c_ℓ are the Fourier coefficient of the periodic function $\tilde{\Psi}_p(x)$. An analogous relation is also valid when the condensate is not in a well-defined Bloch state, but in a superposition of Bloch states of the first band. In this case, the width of the peaks of the momentum distribution will be equal to the width of the quasi-momentum distribution. In the following we will work with the momentum distribution, which is simply obtained from the Fourier transform of the condensate wavefunction.

A. Bloch oscillations

Bloch oscillations can be explained in very simple terms. In the presence of a linear potential superimposed to the optical lattice, the behaviour of a particle with quasi-momentum p is described by the equation of motion $p(t) = Ft$, where F is the constant force due to the linear potential. Since the velocity is given by $v_g = \partial\varepsilon(p)/\partial p$, when the effective mass is negative, the particle will respond to a positive (negative) force with a negative (positive) acceleration. Since the energy band $\varepsilon(p)$ is periodic in p , this will result in periodic oscillations in coordinate and velocity space.

This simple explanation, even neglecting important effects like Landau-Zener tunneling to a higher band, provides a useful model to interpret experiments with electrons [25], with cold atoms [26] and with Bose-Einstein condensates [4,5]. However, if interactions in the condensate play a mayor role, the scenario can change dramatically. First of all, the momentum distribution $\Psi(p, t)$ will not evolve just like $\Psi(p(t))$, as it approximately happens for non interacting systems, but will also spread. Furthermore, in the presence of interactions, it might happen that the condensate gets dephased and, after a short while, the oscillations stop (see Movie 4). For the situation described in the movie

($s = 10$, for which the tight binding approximation works well), the dephasing process begins when the center of the momentum distribution reaches $p = q_B/2$. This point corresponds both to the on-set of the dynamical instabilities and the inversion of the effective mass. Since the momentum distribution has a certain width, one could think that the oscillations stop because the sign of the effective mass is not the same for the whole condensate. An alternative interpretation relies on the onset of dynamical instabilities.

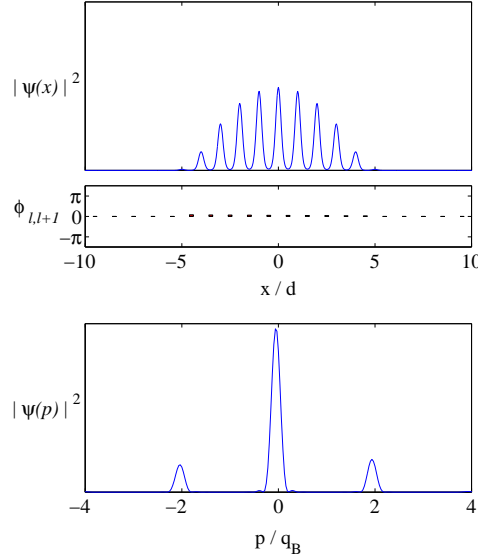


FIG. 4. MOVIE: Bloch oscillations for $s = 10$ and $gn = 0.5E_R$. Time evolution of the spatial density (upper plot), of the relative phases (middle plot) and of the momentum distribution (lower plot).

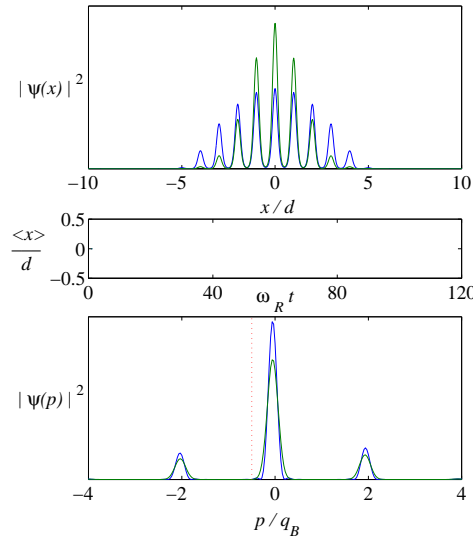


FIG. 5. MOVIE: Bloch oscillations with $s = 10$, $gn = 0$ (green line) and $gn = 0.5E_R$ (blue line). Time evolution of the spatial density (upper plot), of the center of mass (middle plot) and of the momentum distribution (lower plot). The red dotted line indicates the onset of dynamical instabilities in the interacting case.

In order to highlight the correct interpretation, we study the Bloch dynamics of a non interacting condensate, which is always dynamically stable. The initial spatial width is chosen in order to get about the same momentum distribution as in the interacting case, in order to have similar effective mass effects. More specifically, since in the interacting case the width of the momentum distribution increases slowly, while in the non interacting case it remains almost constant, we choose the initial conditions so that the two momentum distributions will be similar at the “critical point”, where $\langle p \rangle = q_B/2$.

The direct comparison is shown in Movie 5. We observe, in the non-interacting case, regular, perfectly periodic Bloch oscillations, in spite of the finite width of the momentum distribution. This clearly shows that, in the interacting case, the onset of decoherence is due to the dynamical instability.

B. Dipole oscillations

Dipole oscillations consist in the motion of the condensate at the bottom of the harmonic trap. The average velocity is periodic in time and the momentum distribution, showing the characteristic peaks due to the optical lattice, also oscillates periodically in time at the bottom of the band. During the time evolution, the phase differences between neighbouring condensates remain locked over the whole condensate.

For a given set of parameters corresponding to small displacements, small interactions or small optical potential depths, dipole oscillations remain periodic, with the condensate locked in phase. Instead, increasing one of these quantities, we find that the oscillations get dephased during the time evolution, or even stop before the condensate reaches the bottom of the harmonic potential. For the seek of comparison we display in Movie 6(a-c) the evolution of the density, of the phase difference and of the momentum distribution for the following sets of parameters. For fixed interactions ($gn = 0.01E_R$) and harmonic trap ($\hbar\omega_x = 0.004E_R$), we choose:

- (a) $s = 3$, $x_0 = 3d$: oscillations;
- (b) $s = 3$, $x_0 = 9d$: broken oscillations;
- (c) $s = 10$, $x_0 = 9d$: broken oscillations.

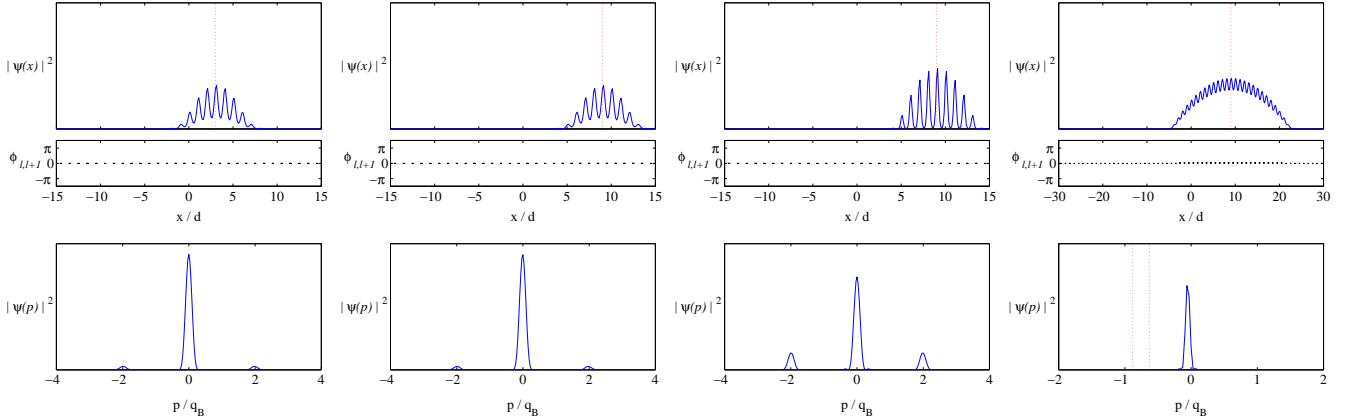


FIG. 6. MOVIES: Dipole oscillations for $gn = 0.01E_R$, $s = 3$, $x_0 = 3d$ (a); $gn = 0.01E_R$, $s = 3$, $x_0 = 9d$ (b); $gn = 0.01E_R$, $s = 10$, $x_0 = 9d$ (c); $gn = 0.5E_R$, $s = 1$, $x_0 = 9d$ (d). Time evolution of the spatial density (upper plot), of the relative phases (middle plot) and of the momentum distribution (lower plot). In movie (d), we indicate with a red dotted line the quasi-momentum where the dynamical instabilities arise and with a green dotted line the quasi-momentum where the effective mass changes sign.

Looking at the phase difference between neighbouring condensates, we find that when the condensate oscillation is interrupted, the phases get scrambled. This corresponds to a randomized flux of atoms which are not able anymore to flow coherently downwards the potential. The evolution of the momentum distribution suggests that this phenomenon happens when the condensate reaches the instability region, given in the specific cases by p greater than $q_B/2$.

To further explore this interpretation, we choose a shallow optical potential such that there is a broad range of p where the effective mass $m_\varepsilon(p)$ is positive and at the same time the system is dynamically unstable (see Fig. 3). We increase the nonlinear interaction parameter to get a relevant imaginary part of the excitation frequencies, otherwise the time scale where instabilities manifest themselves is too long. In Movie 6(d) (lower plot), we indicate with a red dotted line the quasi-momentum where the dynamical instabilities arise and with a green dotted line the quasi-momentum where the effective mass changes sign. We actually observe the first signatures of decoherence when the momentum distribution is contained between the two lines, indicating that the decoherence happens in correspondence of the dynamical instability point. We conclude this section mentioning that experimental evidences of dynamical instabilities are reported in [23].

C. Expansion in the lattice

After creating the condensate in the harmonic trap superimposed to the lattice, we switch off the harmonic trap and let the condensate, which is initially at rest, expand. During the expansion, the current of atoms is from the inside to the outside of the cloud and the phase differences increase, being positive for $x < 0$ and negative for $x > 0$. In [12] the occurrence of self-trapping has been predicted in the tight-binding: when interactions are larger than a critical value, the width of the wave packet does not continue to increase with time (as for vanishing or small interactions) and the wave packet remains localized around a few sites. A similar nonlinear self-trapping occurs in the two-site problem [27].

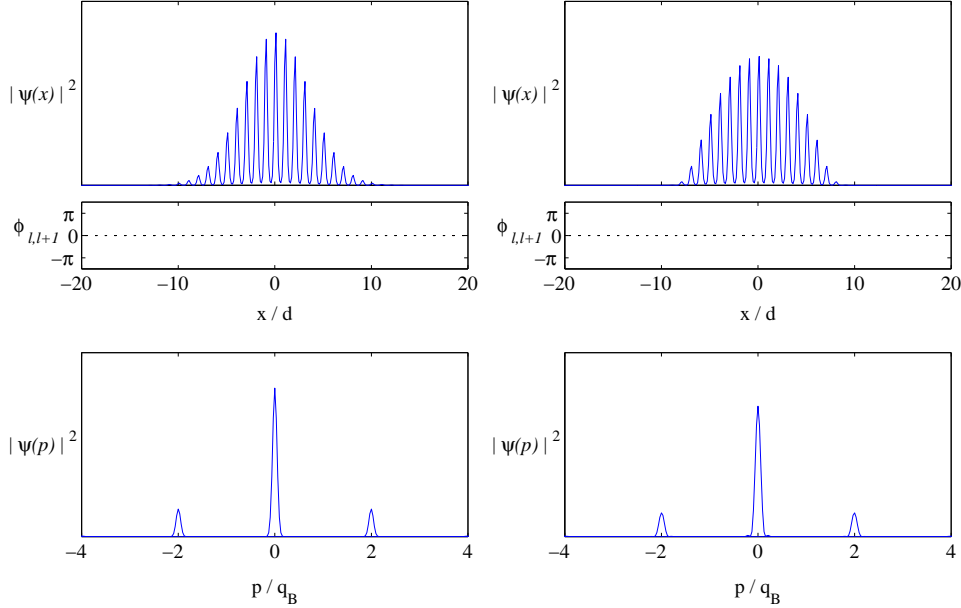


FIG. 7. MOVIES: Expansion of a BEC wave-packet for $gn = 0$, $s = 5$ (a); $gn = 0.01E_R$, $s = 5$ (b); Time evolution of the spatial density (upper plot), of the relative phases (middle plot) and of the momentum distribution (lower plot).

Increasing the interactions, the system enters in the self-trapped regime as shown in Movie 7(b). If interactions are strong enough, we see that after a first stage (whose duration depends on the strength of the interactions) the expansion stops and the condensate evolves as a random flow of atoms between the condensates localized at the bottom of the different potential wells, indicating the onset of a new dynamical instability. In this case, however, a Bogoliubov-like stability analysis is much more problematic because of the non trivial temporal evolution of the condensate wave-packet. A possible, though approximate, approach is to write down an effective Hamiltonian of the system in terms, for instance, of the collective coordinates introduced in Sect.V. Such Hamiltonian would contain a limited number of degree of freedom, making the stability analysis a much easier task. This is the approach followed in [12] to study the dynamics of an expanding condensate in the discrete nonlinear Schrödinger equation framework (with $m_\mu = m_\varepsilon$). Within this approach one recovers, in a unified framework, the critical values of the parameters for the self-trapping conditions of a wavepacket of finite width initially at rest, and the onset of the modulational instability of a Bloch wave discussed in the previous sections. For instance, considering a gaussian wavepacket with initial width σ_0 and quasi-momentum p_0 , the collective coordinates approach predicts the onset of self-trapping at a critical value of the parameter $\Lambda = U_2 N_T / 2K$ [12]. When $\cos(p_0) > 0$, the critical value is $\Lambda_c \approx 2\sqrt{\pi}\sigma_0 \cos(p_0)$; when $\cos(p_0) < 0$, the critical value is $\Lambda_c \approx 2\sqrt{\pi} |\cos(p_0)| / \sigma_0$. We remark that when the width of the wavepacket is very large ($\sigma_0 \rightarrow \infty$), $\Lambda_c \rightarrow \infty$ if $\cos(p_0) > 0$ (and the system is always dynamically stable), while $\Lambda_c \rightarrow 0$ if $\cos(p_0) < 0$ (and the system is always dynamically unstable), recovering the findings of Sect.IV.

The study of the dynamical instabilities of a condensate trapped in an periodic potential is quite a rich problem, and deserves further investigations. As we have mentioned, this is connected to the general problem of the stability of a non stationary state, which includes for instance also the propagation of sound waves in the non linear regime. First experimental results on the self-trapping with weakly coupled BECs are reported in [28,29].

VII. CONCLUSIONS

The Gross-Pitaevskii dynamics of a Bose-Einstein condensate trapped in a deep periodic potential can be studied in terms of a discrete, nonlinear equation. This mapping allows a clear and intuitive picture of the main dynamical properties of the system, which can be calculated analytically. We have calculated the effective masses of the system, connected to the Bloch energy and chemical potential spectra. We have calculated the Bogoliubov dispersion relation, and studied the sound velocity and the appearance of energetic and dynamical instabilities. We have generalized these concepts to the case of shallow optical lattice, which requires a numerical solution and provides complementary insight in the understanding of the problem. Both in the tight binding limit and in the case of shallow optical potential, we have investigated in detail the arising of dynamical instabilities, which seem to be the main mechanism of dephasing of the condensate in Bloch oscillation and dipole oscillations experiments.

Acknowledgements. We thank M. Krämer, L. Pitaevskii and S. Stringari for interesting discussions. This work has been partially supported by the DOE.

Note added in Proofs: An equation similar to the DNL equation (5) has been derived in M. Öster, M. Johansson, and A. Eriksson, Phys. Rev. E **67**, 056606 (2003), to describe the dynamics of an electric field in an array of coupled optical waveguides embedded in a material with Kerr nonlinearities.

-
- [1] M. Greiner, O. Mandel, T. Esslinger, T.W. Hänsch, and I. Bloch, Nature **415**, 39 (2002).
 - [2] S.L. Rolston and W.D. Phillips, Nature **416**, 219 (2002) and refs therein.
 - [3] C. Orzel, A.K. Tuchman, M.L. Fenselau, M. Yasuda, and M.A. Kasevich, Science **291**, 2386 (2001) and refs therein.
 - [4] B.P. Anderson and M.A. Kasevich, Science **282**, 1686 (1998).
 - [5] O. Morsch, J.H. Müller, M. Cristiani, D. Ciampini and A. Arimondo, Phys. Rev. Lett. **87**, 140402 (2001)
 - [6] F.S. Cataliotti, S. Burger, C. Fort, P. Maddaloni, F. Minardi, A. Trombettoni, A. Smerzi, and M. Inguscio, Science **293**, 843 (2001).
 - [7] M.P.A. Fisher, P.B. Weichman, G. Grinstein, and D.S. Fisher, Phys. Rev. B **40**, 546 (1989).
 - [8] D. Jaksch, C. Bruder, J.I. Cirac, C.W. Gardiner, and P. Zoller, Phys. Rev. Lett. **81**, 3108 (1998).
 - [9] K. Berg-Sørensen and K. Molmer, Phys. Rev. A **58**, 1480 (1998).
 - [10] J. Javanainen, Phys. Rev. A **60**, 4902 (1999).
 - [11] M.L. Chiofalo and M.P. Tosi, Phys. Lett. **A268**, 406 (2000).
 - [12] A. Trombettoni and A. Smerzi, Phys. Rev. Lett. **86**, 2353 (2001).
 - [13] F.K. Abdullaev, B.B. Baizakov, S.A. Darmanyan, V.V. Konotop, and M. Salerno, Phys. Rev. A **64**, 043606 (2001); G.L. Alfimov, P.G. Kevrekidis, V.V. Konotop and M. Salerno, Phys. Rev. E **66**, 046608 (2002)
 - [14] A-M Rey, P.B. Blakie and C.W. Clark, Phys. Rev. A **67**, 053610 (2003).
 - [15] B. Wu and Q. Niu, Phys. Rev. A **64**, 061603(R) (2001).
 - [16] A. Smerzi, A. Trombettoni, P.G. Kevrekidis, and A.R. Bishop, Phys. Rev. Lett. **89**, 170402 (2002).
 - [17] M. Machholm, C.J. Pethick, and H. Smith, Phys. Rev. A **67**, 053613 (2003).
 - [18] A. Smerzi and A. Trombettoni, Phys. Rev. A **68**, 023613 (2003); A. Smerzi and A. Trombettoni, Chaos, Focus issue on “Nonlinear localized modes: fundamental concepts and applications”, **13**, 766 (2003).
 - [19] F. Dalfovo, S. Giorgini, L.P. Pitaevskii, and S. Stringari, Rev. Mod. Phys. **71**, 463 (1999).
 - [20] M. Krämer, C. Menotti, L.P. Pitaevskii, and S. Stringari, Eur. Phys. J. D, in press (cond-mat/0305500).
 - [21] M. Machholm, A. Nicolin, C. J. Pethick, H. Smith, cond-mat/0307183.
 - [22] W. Li and A. Smerzi, unpublished.
 - [23] F. S. Cataliotti, L. Fallani, F. Ferlaino, C. Fort, P. Maddaloni, and M. Inguscio, New Journal of Physics **5**, 71 (2003).
 - [24] Yu.S. Kivshar and M. Peyrard, Phys. Rev. A **46**, 3198 (1992).
 - [25] C. Waschke *et al.*, Phys. Rev. Lett. **70**, 3319 (1993).
 - [26] M.B. Dahan *et al.*, Phys. Rev. Lett. **76**, 4508 (1996); S. R. Wilkinson *et al.*, Phys. Rev. Lett. **76**, 4512 (1996).
 - [27] A. Smerzi, S. Fantoni, S. Giovanazzi, and S.R. Shenoy, Phys. Rev. Lett. **79**, 4950 (1997).
 - [28] O. Morsch, M. Cristiani, J.H. Müller, D. Ciampini, and E. Arimondo, Phys. Rev. A **66**, 021601 (2002).
 - [29] M. Oberthaler *et al.*, unpublished.